Computer simulation of a 1.0 GPa piston–cylinder assembly using finite element analysis (FEA)

Sugandha Dogra, Sanjay Yadav *, A.K. Bandyopadhyay

National Physical Laboratory (NPLI), Council of Scientific and Industrial Research (CSIR), New Delhi 110 012, India

A B S T R A C T

The paper reports a preliminary study of the behavior of a high performance controlled-clearance piston gauge (CCPG) in the pressure range up to 1 GPa through finite elemental analysis (FEA). The details of the experimental characterization of this CCPG has already been published (Yadav et al., 2007 [1]). We have already pointed out that the use of Heydemann–Welch (HW) model for the characterization of any CCPG, has some limitation due to the fact that the linear extrapolation of the cube root of the fall rate versus jacket pressure ($v^{1/3}$–p_j) curve is assumed to be independent of the rheological properties of the pressure transmitting fluids. The FEA technique addresses this problem through simulation and optimization with a standard ANSYS program where the material properties of the piston and cylinder, pressure dependent density and viscosity of the pressure transmitting fluid etc. are to be used as the input parameters. Thus it provides characterization of a pressure balance in terms of effective area and distortion coefficient of the piston and cylinder. The present paper describes the results obtained on systematic studies carried out on the effect of gap profile between piston and cylinder of this controlled-clearance piston gauge, under the influence of applied pressure (p) from 100 MPa to 1000 MPa, on the pressure distortion coefficient (λ) of the assembly. The gap profile is also studied at different applied jacket pressure (p_j) such that p_j/p varied from 0.3, 0.4 and 0.5.

1. Introduction

The accurate determination of pressure distortion coefficients (λ) as a function of applied pressure (p), zero pressure effective area (A_0) of piston–cylinder assembly with effective area (A_p) measurement as $A_p = A_0(1 + \lambda p)$ and the associated uncertainties for pressure balances operating at approximately 50 MPa and higher pressures has been carried out by many authors using various methods in high pressure metrology [2–7]. A good agreement has been reported in most of the studies between the theoretical methods. However, discrepancies were observed between the theoretical and the experimental results. The differences were comparatively large in the theoretical and experimental results in case of controlled-clearance piston gauges.

A number of different techniques have been used in the past for the characterization of controlled clearance type piston gauges. Among all these methods, the Heydemann–Welch (HW) model, is widely accepted and used by some of the national metrological laboratories [1,8–17] but has some limitation due to the fact that the linear extrapolation of the cube root of the fall rate versus jacket pressure ($v^{1/3}$–p_j) curve is assumed to be independent of the rheological properties (density and viscosity) of the pressure transmitting fluids. The technique based on FEA has been specifically tailored to model piston–cylinder gap profile, pressure distortion, related pressure gradients and flow of the operating fluid. Samman [18], Samman and Abdullah [19], Sabuga [20], Molinar et al. [21], Buonanno et al. [22,23] are the researchers who initiated to use FEA as a tool to study the different designs of p–c

assemblies. The most recent studies carried out by Molinar et al. [24,25] and Sabuga et al. [26,27] are the example to prove that FEA is a sensitive and powerful tool for such analysis and addresses amicably the problem faced in HW model through simulation and optimization with a standard ANSYS program where the material properties of the piston and cylinder, pressure dependent density and viscosity of the pressure transmitting fluid etc. are used as the input parameters. Thus it provides characterization of a pressure balance in terms of effective area and distortion coefficient of the piston and cylinder.

The National Physical Laboratory of India (NPLI), New Delhi used the HW model to establish and realize its national practical pressure scale up to 5 MPa in pneumatic pressure range [12]; 500 MPa [13–15] and most recently extended up to 1 GPa [1] in hydraulic pressure range. The present paper reports a preliminary study of the behavior of a high performance controlled-clearance piston gauge (CCPG) (nominal diameter of 2.5 mm) in the pressure range up to 1 GPa through FEA. The initial findings of the studies were reported elsewhere [28]. The systematic studies thus carried out on the effect of applied pressure (p) from 100 MPa to 1000 MPa on the gap profile between piston and cylinder, pressure distortion coefficient (λ) of the assembly using FEA are reported. The gap profile is also studied at different applied jacket pressure (p_j) such that p_j/p varied from 0.3, 0.4 and 0.5. The results thus obtained using FEA are compared with the experimental values.

2. Description of the 1 GPa CCPG piston–cylinder assembly

The details of the 1 GPa piston–cylinder assembly are reported in our earlier paper [1]. It is a NPLI national primary hydraulic pressure standard in the pressure range 100–1000 MPa. A schematic diagram of the assembly is shown in Fig. 1. The diameter of the piston measured with the help of NPLI Reference Standard Slip Gauge within the measurement uncertainty of ±0.06 μm ($k = 2$), is 2.52283 mm. The inner and outer diameters of the cylinder measured by Precision 3D Coordinate Measuring Machine within the uncertainty limit ± (0.8 + L/900) μm ($k = 2$), are 2.5247 mm and 26.0223 mm, respectively. This corresponds to the initial clearance width $h = 0.935$ μm. In the free deformation mode (FDM), these dimensions of the piston and cylinder were taken into consideration for computation using FEA. In the controlled clearance mode (CCM), the jacket pressure (p_j) is applied such that p_j/p varied from 0.3, 0.4 and 0.5 to the outer surface of the cylinder as shown in the diagram. The piston is made of tungsten carbide and cylinder is made of steel. The values of Young moduli, $E_p = 620.58$ GPa, $E_c = 206.84$ GPa, Poisson ratio, $\mu_p = 0.218$, $\mu_c = 0.285$, and thermal expansion coefficients, $\alpha_p = 4.42 \times 10^{-6}/°C$, $\alpha_c = 10.5 \times 10^{-6}/°C$, reported by the manufacturer are used in computation. The piston is in floating position when it is located 3.4 mm above its rest position in the cylinder. The total engagement length is 18.9 mm.

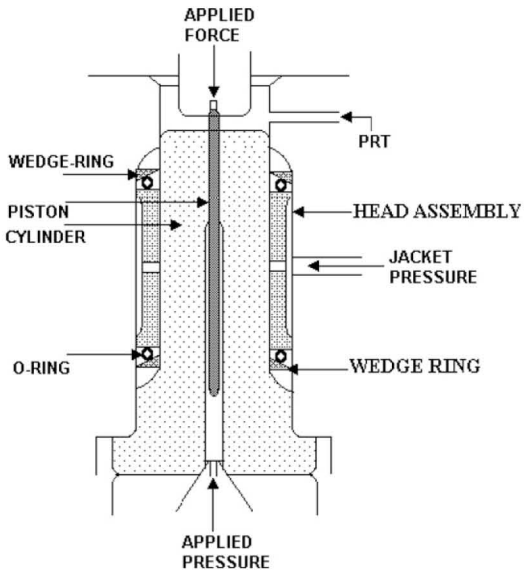

Fig. 1. Schematic diagram of the piston–cylinder assembly.

3. Modelling of piston–cylinder assembly for FEA analysis

The structural problem of the p–c assembly was solved both in FDM and CCM using ANSYS software version 9.0 finite element program. A two dimensional model of the p–c assembly is considered assuming p–c assembly as axially symmetric as shown in Fig. 2. The x–y coordinates of all the keypoints thus created are shown in Table 1.

The areas of the axially symmetric piston and cylinder were formed from these keypoints. These areas were then meshed with 2416 (eight nodes) quadrilateral elements

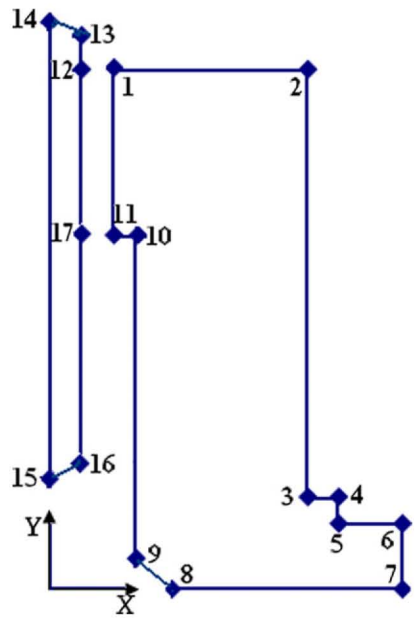

Fig. 2. Keypoints created for the modelling assuming p–c assembly as axially symmetric in a two dimensional model.

Table 1
x–y Coordinates of piston–cylinder keypoints.

Keypoints	*x* (mm)	*y* (mm)
Cylinder		
1	1.26235	59.55
2	13.01115	59.55
3	13.01115	10.55
4	15	10.55
5	15	7.5
6	19.1	7.5
7	19.1	0
8	3.8	0
9	1.86235	4.60923
10	1.86235	40.65
11	1.26235	40.65
Piston		
12	1.261415	59.55
13	1.261415	61.525
14	0	62.95
15	0	12.55
16	1.261415	13.975
17	1.261415	40.65

and 2768 nodes of smart size 4. There were total 254 nodes created along the engagement length of 18.9 mm between keypoints 12–17 of piston and 1–11 of cylinder. A uniform pressure equal to measured pressure, p, was applied to the lines 9–10, 10–11, 15–16 and 16–17. The movement of the piston and cylinder were restricted by applying constraints in y direction to the lines 1–2, and 13–14. In case of CCM, additional load equal to jacket pressure, p_j, was applied to the lines 2–3. The segment along the engagement length was exposed to a linearly varied pressure values obtained using hydrodynamic calculations. FEA calculations were performed at the reference temperature of 20 °C and for the pressures 20 MPa, 100 MPa, 200 MPa, 300 MPa, 400 MPa, 500 MPa, 600 MPa, 700 MPa, 800 MPa, 900 MPa and 1 GPa.

The di(2-ethylhexyl) sebacate (also known as BIS commercially) is used as pressure transmitting fluid. The density (ρ, kg/m^3) and dynamic viscosity (η, Pa s) of BIS as a function of pressure (p, MPa) (p is linearly variable pressure) at 20 °C were calculated using the following equations derived by Molinar [29] from the experimental data from [30] for $p \leqslant 500$ MPa and [31] for $p > 500$ MPa $\leqslant 1$ GPa:

$$\rho\ (\mathrm{kg/m^3}) = 912.67 + 0.752p - 1.645 \times 10^{-3} \cdot p^2 + 1.456 \times 10^{-6} \cdot p^3\ (p \leqslant 500\ \mathrm{MPa}) \quad (1)$$

$$\rho\ (\mathrm{kg/m^3}) = 915.61 + 0.505727p - 0.661573 \times 10^{-3} \cdot p^2 + 0.584283 \times 10^{-6} \cdot p^3 - 0.204436 \times 10^{-9} \cdot p^4\ (p > 500\ \mathrm{MPa} \leqslant 1\ \mathrm{GPa}) \quad (2)$$

$$\eta\ (\mathrm{Pa\ s}) = 0.021554 \times (1 + 1.90036 \times 10^{-3} \cdot p)^{8.8101}\ (p \leqslant 500\ \mathrm{MPa}) \quad (3)$$

$$\eta\ (\mathrm{Pa\ s}) = 459.968 - 4.93208 \cdot p + 0.0213348 \cdot p^2 - 4.8768 \times 10^{-5} \cdot p^3 + 6.25155 \times 10^{-8} \cdot p^4 - 4.28033 \times 10^{-11} \cdot p^5 + 1.2575 \times 10^{-14} \cdot p^6\ (p > 500\ \mathrm{MPa} \leqslant 1\ \mathrm{GPa}) \quad (4)$$

4. Theoretical aspects

The mechanical theory of elastic equilibrium allows determination of the elastic distortion of the piston and cylinder from the pressure distribution in the clearance. Such distortions are obtained using the elastic equilibrium conditions on the piston–cylinder assembly. Assuming the hypothesis of constant clearance, one can use simplified relationship to evaluate the pressure distortion coefficient, as reported in [6]. In case of the gap profiles depend upon the axial coordinates, the effective area, A_p, of a piston–cylinder assembly is determined as follows [2,6]:

$$A_p = \pi r_p^2(0)\left[1 + \frac{h(0)}{r_p(0)} + \frac{1}{(p_1 - p_2)r_p[0)} \int_0^l [(U(z) + u(z)]\frac{dp_z}{dz}dz\right] \quad (5)$$

where $r_p(0)$ is the radius of undistorted piston at axial coordinate, $z = 0$, $h(0)$ is the initial gap width between undistorted piston and cylinder, p_z is the pressure distribution in the clearance, $U(z)$ and $u(z)$ are the radial displacements of the cylinder and piston, respectively.

The method used for the computation of distortion coefficient is identical as used in [27] which is based on the solution of the structural and fluid flow problems assuming the flow between piston and cylinder to be axial, hydrostatic, one dimensional, Newtonian viscous, isothermal and laminar. In such a case, the relationship between pressure distribution in the clearance, gap profile, $h(z)$ and the rheological properties of the pressure transmitting fluid is determined by the solution of the Navier–Strokes equation and the equation of continuity as follows [6,18,23,27]:

$$p_z = p + k\int_0^z \frac{\eta(p)}{\rho(p)} \cdot \frac{1}{h^3(z)}dz \quad (6)$$

where k is given by:

$$k = -p \Big/ \int_0^l \frac{\eta(p)}{\rho(p)} \cdot \frac{1}{h^3(z)}dz \quad (7)$$

where $\eta(p)$ and $\rho(p)$ are the dynamic viscosity and density of the pressure transmitting fluid, respectively. Eqs. (6) and (7) were integrated using Simpson's method to obtain their solutions. Since $\eta(p)$, $\rho(p)$ and k are function of the pressure distribution in the gap, p_z is computed using iterative approach, reported in the literature [23]. At the first iteration, a linear pressure profile is applied along the gap from p to zero and, then, the corresponding k value is obtained using (7). The obtained k value is then replaced in (6) together with the fluid properties, leading to a new pressure distribution p_z to be applied for the next iteration. The pressure distribution thus computed in the gap for a particular applied pressure, p, is then curve fitted using Fourier Transformation in a separate software platform named Origin 6.1 to minimize the integration errors. The final values of the pressure distribution thus calculated are then fed into the FEA program to calculate the elastic distortions and the new gap profile.

The effective area, A_p is then computed form the values of R_p, r_p and p_z using (5). The pressure distortion coefficient is then computed as follows:

$$\lambda = \{(A_p/A_0) - 1\}/p \tag{8}$$

where A_0 is the zero pressure effective area and is computed using:

$$A_0 = \pi r_p^2(0)\left[1 + \frac{1}{r_p(0)} \cdot \frac{\int_0^l \frac{1}{h^2}dz}{\int_0^l \frac{1}{h^3}dz} + \frac{2}{r_p(0)} \cdot \frac{\frac{\int_0^l r_p - r_p(0)}{h^3}}{\int_0^l \frac{1}{h^3}dz}\right] \tag{9}$$

5. Results and discussion

The meshed deformed structure of piston–cylinder assembly used in CCM is shown in Fig. 3a for whole assembly. Fig. 3b shows the zoom portion of the engagement length at an applied pressure of 1.0 GPa in CCM at a p_j = 0.5 of p. The normalized pressure distribution p_z along the normalized axial coordinate, z in the engagement length of piston–cylinder, computed using (6) and (7) is shown in Fig. 4. The dimensionless axial coordinate, z is defined as axial engagement length of the piston–cylinder engagement length as z = 0 mm (initial length) to z = 18.9 mm (final length). The gap width affects the pressure distribution and it is nearly linear near the bottom due to the decrease in pressure gradient there. However, the linear behavior changes approaching towards top and it becomes near to parabolic shape for the applied pressures. Fig. 4 shows that p(z) in the gap depends upon the measured pressure, p and it shows, as usual, as nearly linear (at lower p) to marked non-linearity that increases with increase in measured pressure p.

For the computation of p(z), the pressure dependence of density, $\rho(p)$ and viscosity, η(p) of sebacate oil was considered

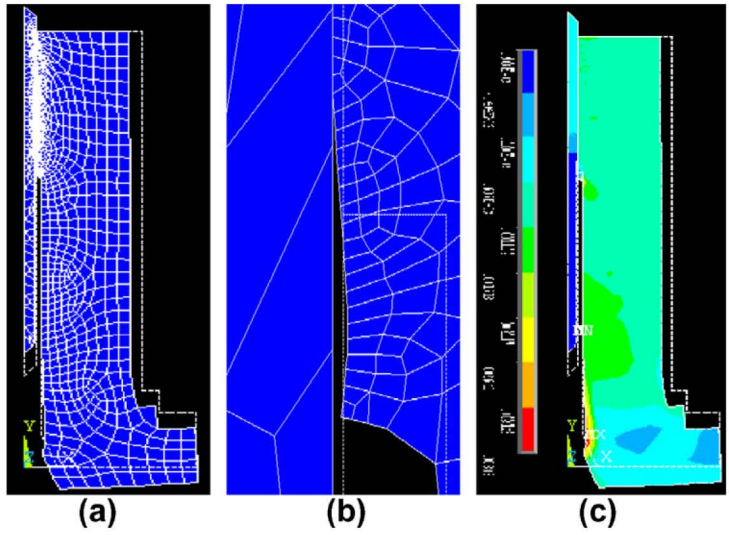

Fig. 3. (a) Meshed deformed structure of p–c assembly, (b) meshing around engagement length and (c) image of the distorted p–c assembly in CCM mode at p = 1.0 GPa and p_j = 0.5 p.

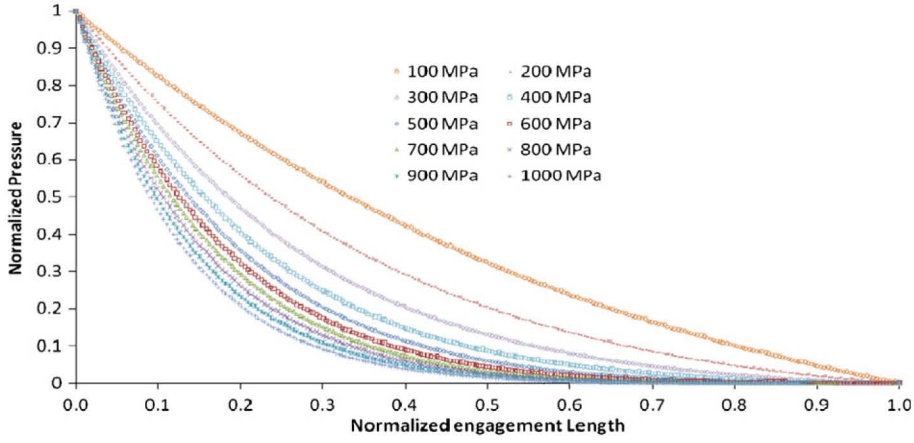

Fig. 4. Normalized pressure distributions in the clearance as a function of normalized length for different applied pressures.

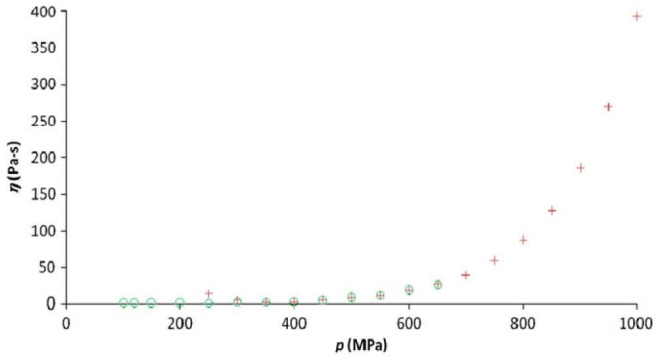

Fig. 5. Pressure dependent of viscosity $\eta(p)$ of pressure transmitting fluid.

utilizing (1) and (3) for pressure up to ⩽500 MPa and (2) and (4) for pressure > 500 MPa and up to 1000 MPa, respectively. In order to obtain optimum results when changing (3) to (4) for viscosity, we have plotted the calculated values of η(p) as a function of p in Fig. 5.

It is clear from the curves that the values of η(p) are almost superimposed at 400 MPa. Therefore, the use of (3) would give optimum results for pressure ⩽ 500 MPa and (4) for pressure > 500 MPa. It is also clear that any of these two equations can be used for entire pressure range 100–1000 MPa. Even after taking care of this aspect while changing the equations, there is still different patterns of curves obtained for pressures </> 500 MPa which is probably due to the fact that p(z) is not much affected by η(p) for pressure less than 500 MPa.

As mentioned earlier, the gap profile of the piston–cylinder assembly is studied at different varied jacket pressure such that $p_j/\ p = 0$ in FDM and $p_j/\ p = 0.3$, 0.4 and 0.5 in CCM. The results thus obtained on the gap profile of the piston and cylinder generatrix surfaces as a function of normalized engagement length for different applied pressure, p from 100 MPa to 1000 MPa are shown in Fig. 6a–d. The decrease at the top and increase approaching towards bottom in the gap width is clearly visible as the applied pressure, p increases, especially in FDM (Fig. 6a). In FDM, the initial gap of 0.935 μm at $p = 0$ deceases to 0.5 μm at top and increases to 9.5 μm at bottom at $p = 1000$ MPa. However, in CCM, the gap width is found always increasing form top ($l = 18.9$ mm) to bottom ($l = 0$) for all the pressures which is obvious due to the pressure distribution in the gap profile which is equal to atmospheric pressure at top and increases equal to the applied pressure at the bottom.

We have already reported in our previous paper [1] that the piston fall rate for low jacket pressure ($p_j \not\leftarrow 0$ (1 p to 0.2 ψp) is so fast that it cannot be measured with the same reproducibility as has been done with the other points from ($p_j \not\leftarrow 0$ (3 ψp to 0.64 ψp). The reason for fast fall rate is quite evident from the measurement of gap width along the engagement length using FEA. Due to the quite high gap width in FDM and also at lower jacket pressures ($p_j \not\leftarrow 0$ (1 ψp to 0.2 ψp), the floating time of the piston is very low (few seconds) and it is not possible with this CCPG design to measure fall rate/pressure without applying jacket pressure. As expected, the clearance between piston and cylinder decreases as p_j increases.

A small bump is seen in all the curves at $l = 5.3$ mm as is evident from Fig. 6. This bump may be due to the geometrical shape of the assembly and the resultant strains which are also visible in the image of distorted p–c assembly obtained from FEM (Fig. 3c). Also, a small convex curvature is seen in all the curves of Fig. 6 at the beginning part of the engagement length. This may be understood due to the fact that the gap width decreases at the beginning part in comparison to its top part of the engagement length. From this point downwards the cylinder bore diameter is much higher in comparison to along the engagement length. Due to this geometrical edge (Fig. 3b) at the beginning part of the engagement length, the point pressure is applied form all the directions which creates comparatively higher deformation in the cylinder at the beginning part in comparison to the top. In order to study the effect of p_j on gap width, the difference of gap width between FDM and CCM as a function of applied p_j along the engagement length is plotted in Fig. 7. Interestingly, the difference in gap width is almost uniform along the engagement length for all the applied jacket pressures, i.e. $p_j = 0.3\ p$, $0.4\ p$ and $0.5\ p$.

It is clearly evident form Fig. 6 that jacket pressure, p_j affects not only the distortion of cylinder but also of the piston. However, the piston is less sensitive to p_j in comparison to cylinder. The piston distortion is much higher at the top in comparison to bottom. This phenomenon can easily be understood with the fact that the difference in pressure distributions in the clearance for FDM and CCM is higher at the bottom and lower at the top.

The radii of piston and cylinder plotted as a function of normalized engagement length for both FDM and CCM are shown in Fig. 8 for applied pressure of 100 MPa and 1000 MPa.

Fig. 9 shows the effective area (A_p) at 20 °C plotted as a function of jacket pressure, p_j at different nominal pressures p. Linearity of the plots clearly suggests the close agreement between the values of A_0 computed in FDM and the values obtained form the interpolation of curves p_j–A_p in CCM. p_j–A_p curves are also used to determine the values of jacketed distortion coefficient, d of the cylinder using the relation: $d = \{(\Delta A_p/\Delta p_j)/A_p\}$. The average value of d is found to be $3.6 \times 10^{-6}\ \mathrm{MPa}^{-1}$ with measurement uncertainty $3.3 \times$

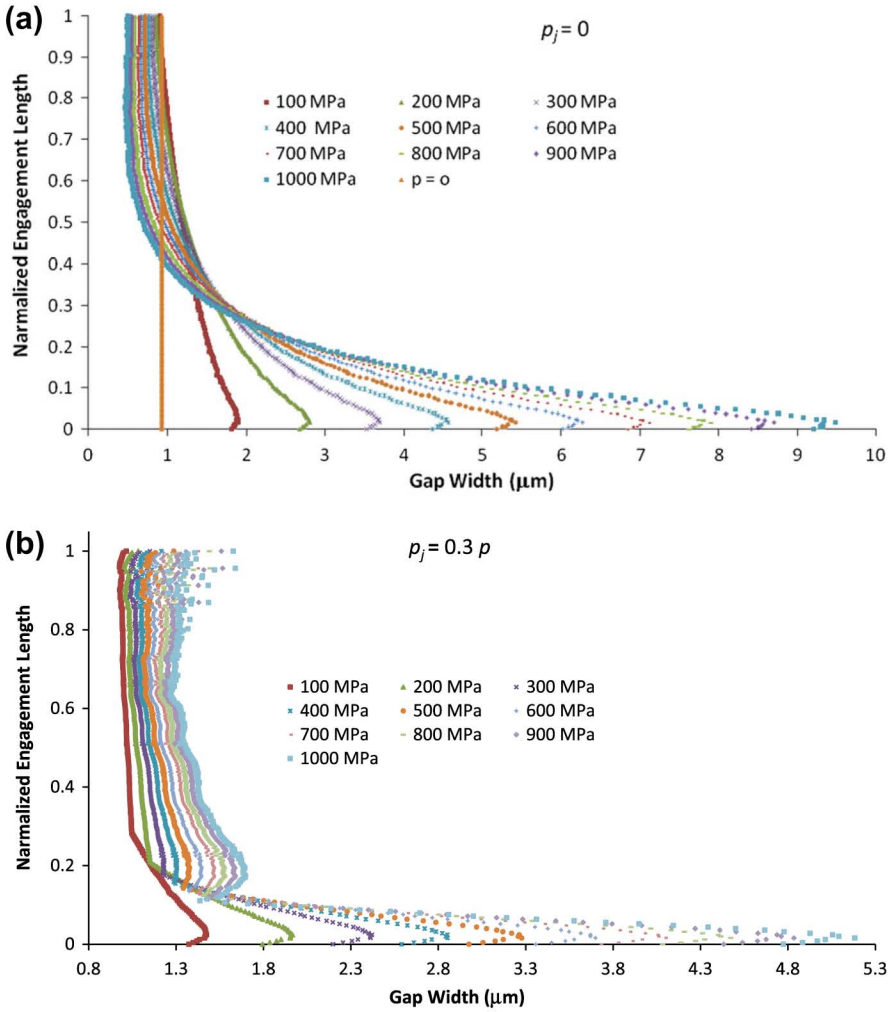

Fig. 6. Gap profile of *p–c* assembly along the engagement length (a) $p_j = 0$ in FDM and (b) $p_j = 0.3\ p$ in CCM, (c) $p_j = 0.4\ p$ in CCM and (d) $p_j = 0.5\ p$ in CCM.

10^{-7} MPa^{-1}. The *d* value varies 1.8–5.4 × 10^{-6} MPa^{-1}. The theoretical '*d*' value is also estimated from dimensional measurements of piston–cylinder assembly using the relationship suggested by Newhall et al. [16] as follows:

$$d = \frac{1}{m \cdot E_c}\left[k - \left(\frac{3\mu_p - 1}{2}\right) \times \frac{E_c}{E_p}\right] \tag{10}$$

where E_p, μ_p and E_c, μ_p are the Young's Modulus and Poisson ratios of piston and cylinder materials, respectively.

m is defined by:

$$m = \frac{(1-\mu_c) + (1+\mu_c)\varpi^2}{2\varpi^2} + \frac{(1-3\mu_p)(\varpi^2 - 1)}{4\varpi^2} \cdot \frac{E_c}{E_p} \tag{11}$$

where ϖ is the ratio of the outer to inner diameter of the cylinder and the constant *k* is estimated using:

$$k = \frac{1}{2}\left[\frac{(\varpi^2 + 1)}{(\varpi^2 - 1)} + \mu_c\right] \tag{12}$$

The value of '*d*' thus calculated as 5.084 × 10^{-6} MPa^{-1}, is quite comparable to the values calculated through FEM, analysis. The average *d* value determined experimentally up to 500 MPa is 6.7 × 10^{-6} MPa^{-1} which varies 3.2–9.8 × 10^{-6} MPa^{-1}. Admittedly, there is some inconsistency in the experimental and FEM *d* values which would be further studied in our future endeavors.

The effective area (A_p) is also plotted as a function of applied pressures *p* in FDM at $p_j = 0$ and in CMM at $p_j = 0.3\ p$, $0.4\ p$ and $0.5\ p$ (Fig. 10). The effective area deceases with increase in p_j and becomes almost uniform at $p_j = 0.5\ p$.

The values of pressure distortion coefficients calculated using (8) from the values of A_p obtained through FEA at different pressures with varying p_j/p as 0 in FDM and 0.3, 0.4 and 0.5 in CCM are shown in Fig. 11. Generally, the pressure distortion coefficient, λ is independent of applied pressure. As expected, the values of λ are much higher in FDM in comparison to CCM. In FDM, the λ varies from minimum 3.08 × 10^{-6} MPa^{-1} to maximum 3.4 × 10^{-6} MPa^{-1} having average value as 3.28 × 10^{-6} MPa^{-1}with measurement uncertainty 0.031 × 10^{-6} MPa^{-1}. The λ is found to decrease with increase in p_j. Similarly, the average values of the λ in CCM are found be 1.06 × 10^{-6} MPa^{-1} ± 0.005 × 10^{-6} MPa^{-1}, 0.68 × 10^{-6} MPa^{-1} ± 0.22 × 10^{-6} MPa^{-1}and

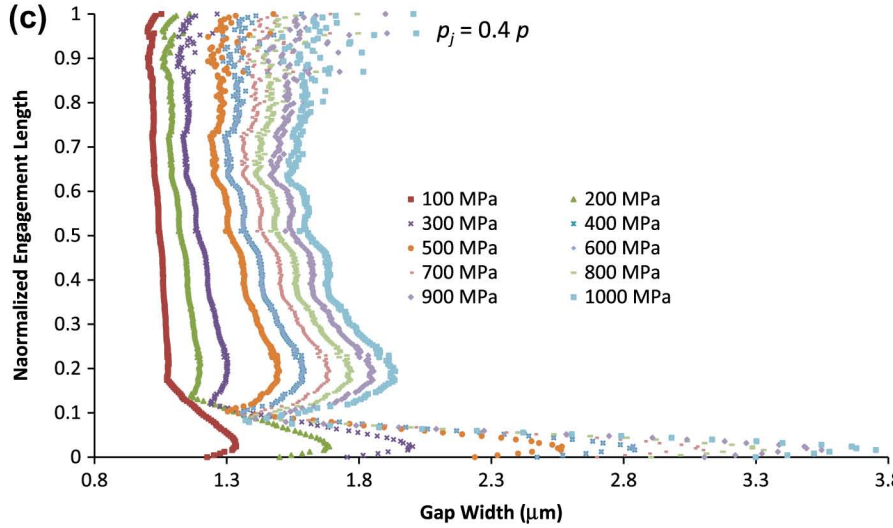

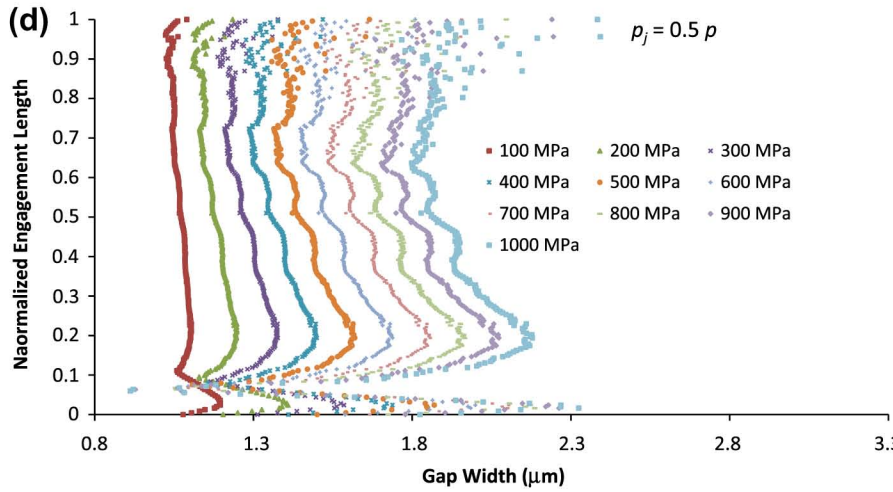

Fig. 6 (*continued*)

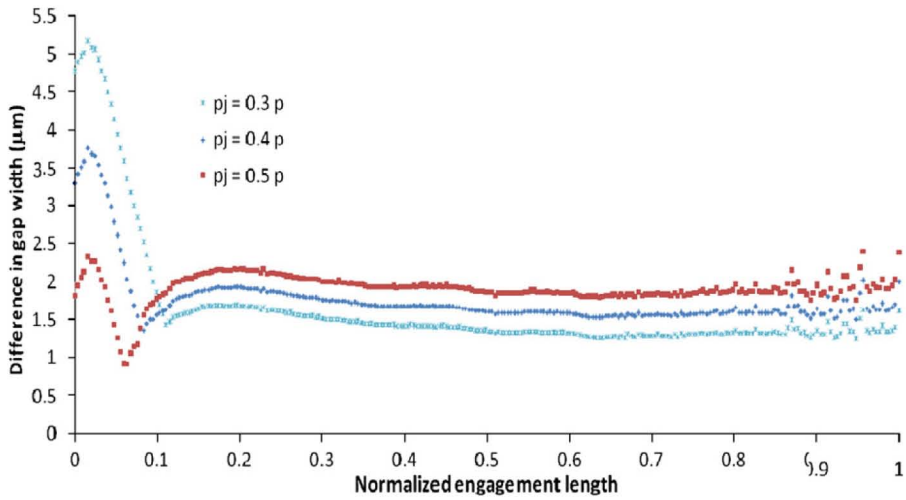

Fig. 7. The difference of gap width between FDM and CCM as a function of applied p_j along the engagement length.

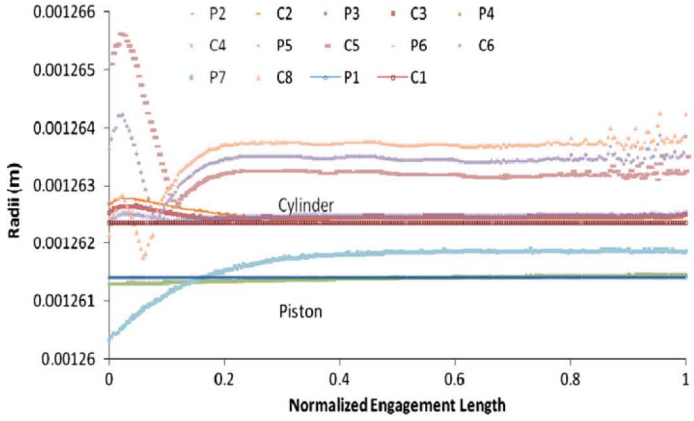

Fig. 8. Radii of piston and cylinder along the engagement length, both in FDM and CCM to show the radial distortions (P1 is at $p = 0$ and $p_j = 0$ for piston, C1 is at $p = 0$ and $p_j = 0$ for cylinder, P2, P3 and P4 are at $p = 100$ MPa and $p_j = 30$ MPa, 40 MPa and 50 MPa pressure, respectively for piston, C2, C3and C4 are at $p = 100$ MPa and $p_j = 30$ MPa, 40 MPa and 50 MPa pressure, respectively for cylinder. Similarly, P5, P6 and P7 are at $p = 1000$ MPa and $p_j = 300$ MPa, 400 MPa and 500 MPa pressure, respectively for piston, C5, C6 and C8 are at $p = 1000$ MPa and $p_j = 300$ MPa, 400 MPa and 500 MPa pressure, respectively for cylinder).

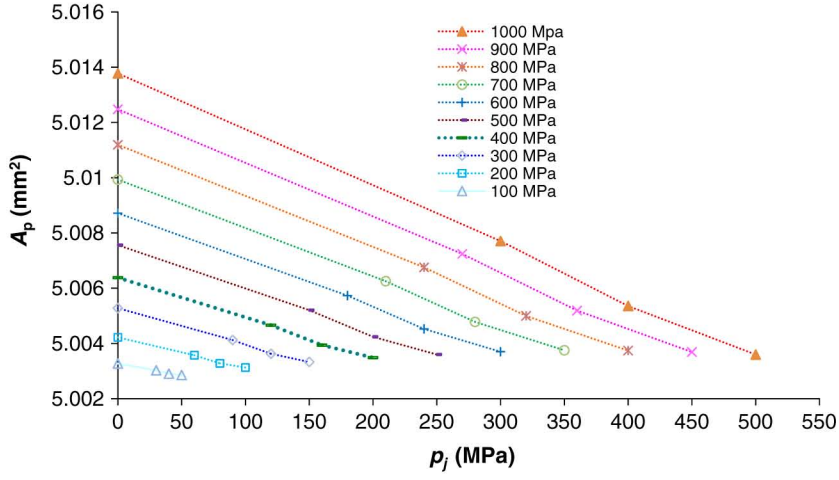

Fig. 9. Effective area, A_p determined for different applied pressures p from 100 MPa to 1000 MPa with p_j/p varying as 0 in FDM and 0.3, 0.4 and 0.5 in CCM.

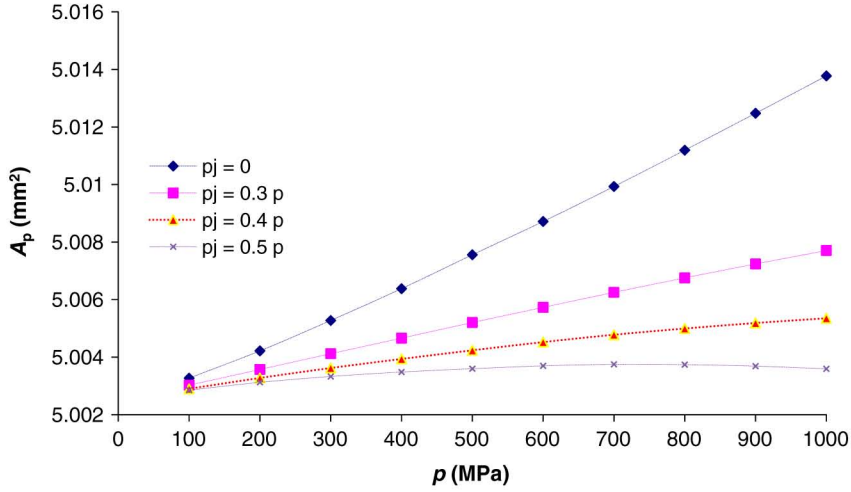

Fig. 10. Effective area, A_p determined as a function of applied pressures p with p_j/p varying as 0 in FDM and 0.3, 0.4 and 0.5 in CCM.

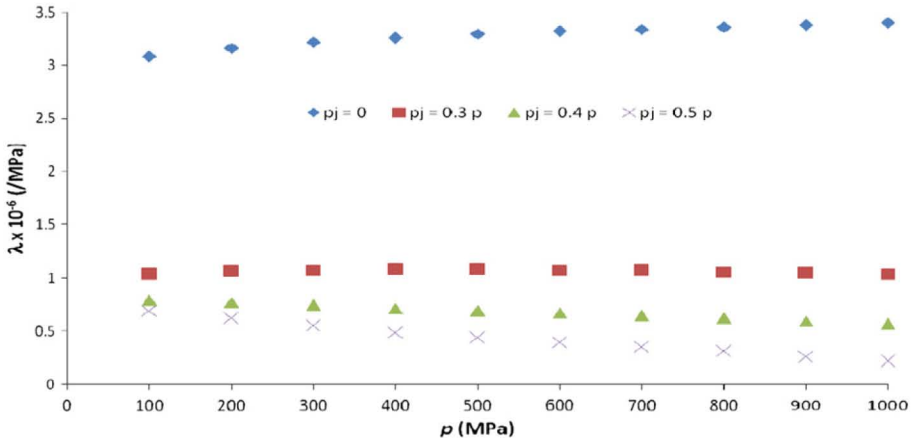

Fig. 11. Distortion coefficient, λ determined as a function of applied pressures p with p_j/p varying as 0 in FDM and 0.3, 0.4 and 0.5 in CCM.

$0.43 \times 10^{-6}\,\mathrm{MPa}^{-1} \pm 0.046 \times 10^{-6}\,\mathrm{MPa}^{-1}$ with p_j/p varying as 0.3, 0.4 and 0.5, respectively.

6. Conclusions

The following conclusions are drawn from the studies:

- A numerical methodology based on the FEA has been used to study the gap profile, pressure distribution in the clearance, pressure distortion coefficient, and effective area of a controlled-clearance piston gauge both in the free deformation and controlled clearance modes.
- The gap width increases with increase in the applied pressure p both in FDM and CCM. At 1.0 GPa, the initial gap of approximately 0.953 μm at $p = 0$ increases to 9.5 μm. The radial clearance gap is always higher than the undistorted value. The change in gap width also increases along the engagement length from top to bottom due to the increase in pressure distribution in the gap profile.
- The jacket pressure, p_j affects not only the distortion of cylinder but also of the piston. However, the piston is less sensitive to p_j in comparison to cylinder. The piston distortion is much larger at the outlet in comparison to inlet.

References

[1] Sanjay Yadav, O. Prakash, V.K. Gupta, A.K. Bandyopadhyay, The effect of pressure transmitting fluids in the characterization of a controlled clearance piston gauge up to 1 GPa, Metrologia 44 (2007) 222–233.

[2] R.S. Dadson, R.G.P. Greig, A. Horner, Development in accurate measurement of high pressures, Metrologia 1 (1965) 55–67.

[3] P.L.M. Heydemann, W.E. Welch, Piston gauges, in: B. Leneindre, B. Voder (Eds.), Experimental Thermodynamics, vol. 2, Butterworth, London, 1975, p. 147.

[4] R.S. Dadson, S.L. Lewis, G.N. Peggs, The Pressure Balance: Theory and Practice, Her Majesty's Stationery Office, London, 1982.

[5] F. Pavese, G.F. Molinar, Modern Gas based Temperature and Pressure Measurements, Plenum, New York, 1994.

[6] G.F. Molinar, R. Maghenzani, P.C. Cresto, L. Bianchi, Elastic distortions in piston cylinder unit at pressures up to 0.5 GPa, Metrologia 29 (1992) 425–440.

[7] J.C. Legras, Pressure distortion coefficient of pressure balances, in: A.K. Bandyopadhyay et al. (Eds.), Advances in High Pressure Science and Technology, NPL, New Delhi, 2001, pp. 9–14.

[8] D.H. Newhall, I. Ogawa, V. Zilberstein, Recent studies of float and stall curves in controlled clearance dead weight testers with a simple piston, Rev. Sci. Instrum. 50 (1979) 964–968.

[9] J.K.N. Sharma, K.K. Jain, V.E. Bean, B.E. Welch, R.J. Lazos, Effects of viscosity, temperature, and rate of rotation on pressure generated by a controlled clearance piston gauge, Rev. Sci. Instrum. 56 (4) (1984) 563–569.

[10] A.K. Bandyopadhyay, P. Hilsch, J. Jager, Use of controlled clearance balances with highly viscous pressure transmitting media, PTB-Mitteilungen 97 (1987) 264–269.

[11] H. Kajikawa, K. Ide, T. Kobata, Precise determination of the pressure distortion coefficient of new controlled clearance piston–cylinders based on the Heydemann–Welch model, Rev. Sci. Instrum. 80 (5) (2009) 095101–095110.

[12] J.K.N. Sharma, K.K. Jain, A.K. Bandyopadhyay, Characterization of a controlled clearance piston gauge using different working fluids up to 5 MPa, Jpn. J. Appl. Phys. 27 (1988) 843–848.

[13] A.K. Bandyopadhyay, A.C. Gupta, Realization of a national practical pressure scale for pressures up to 500 MPa, Metrologia 36 (1999) 681–688.

[14] Sanjay Yadav, V.K. Gupta, A.K. Bandyopadhyay, Characterisation of controlled clearance pressure balance for hydrostatic pressure measurements up to 500 MPa, in: Proc. NSCL Conf., Tampa, FL, 17–18 August 2003, pp 1–16.

[15] A.K. Bandyopadhyay, S. Yadav, N. Dilawar, Current status of pressure standards at NPLI and our experiences with the key comparison data base (KCDB), MAPAN—J. Metrology Soc. India 21 (2006) 127–145.

[16] D.H. Newhall, W.C. Newhall, T. Malloy, Revised characterisation of the controlled clearance piston gauge, Rev. Sci. Instrum. 74 (5) (2003) 2899–2910.

[17] A.K. Bandyopadhyay, D.A. Olson, Characterization of a compact 200 MPa controlled clearance piston gauge as a primary pressure standard using the Heydemann and Welch method, Metrologia 43 (2006) 1–10.

[18] N.D. Samaan, Mathematical Modeling of Instruments for Pressure Measurement, Ph.D. Thesis, City University, London, UK, 1990, p.145.

[19] N.D. Samaan, F. Abdullah, Characterisation of a 1 GPa piston–cylinder unit, Measurement 23 (1998) 179–183.

[20] W. Sabuga, Elastic distortion calculations at PTB on LNE 200 MPa pressure balance as part of EUROMET Project 256, PTB Bericht, Braunschweig, PTB-W-63, 1995.

[21] G.F. Molinar, W. Sabuga, G. Robinson, J.C. Legras, Comparison of methods for calculating distortion in pressure balances up to 400 MPa—EUROMET Project 256, Metrologia 35 (1998) 739–759.

[22] G. Buonanno, M. Dell'Isola, R. Maghenzani, Finite elements analysis of pressure distortion coefficient and piston fall rate in a simple pressure balance, Metrologia 36 (1999) 579–584.

[23] G. Buonanno, M. Dell'Isola, G. Lagulli, G.F. Molinar, A finite element method to evaluate the pressure distortion coefficient in pressure balances, High Temp.–High Press. 31 (1999) 131–143.

[24] G. Molinar, M. Bergoglio, W. Sabuga, P. Otal, G. Ayyildiz, J. Verbeek, P. Farar, Calculation of effective area A_0 for six piston–cylinder assemblies of pressure balances. Results of the EUROMET Project 740, Metrologia 42 (2005) S197–S201.

[25] G. Molinar, G. Buonanno, G. Giovinco, P. Delajoud, R. Haines, Effectiveness of finite element calculation method (FEM) on high performance pressure balances in liquid media up to 200 MPa, Metrologia 42 (2005) S207–S211.
[26] W. Sabuga, G. Molinar, G. Buonanno, T. Esward, T. Rabault, L. Yagmur, Calculation of the distortion coefficient and associated uncertainty of PTB and LNE 1 GPa pressure balances using finite element analysis—EUROMET Project 463, Metrologia 42 (2005) S202–S206.
[27] W. Sabuga, G. Molinar, G. Buonanno, T. Esward, J.C. Legras, L. Yagmur, Finite element method used for calculation of the distortion coefficient and associated uncertainty of a PTB 1 GPa pressure balance—EUROMET Project 463, Metrologia 43 (2006) 311–325.
[28] Sanjay Yadav, A. Lodh, S. Dogra, A.K. Bandyopadhyay, Characterisation of a controlled clearance piston gauge (CCPG) using finite element analysis, in: Proceedings 7th International Conference on Advances in Metrology (AdMet-2009), New Delhi, February 18–20, 2009, pp. 114–115.
[29] G.F. Molinar, Density and dynamic viscosity versus pressure, up to 1 GPa, for the di(2)-ethyl-hexyl-sebacate fluid at 20 °C—EUROMET Project Number 463, Rapporto Tecnico Interno R 486 CNR-IMGC, Torino, December 1998.
[30] P. Vergne, New high pressure viscosity measurements on di(2-ethylhexyl) sebacate and comparison with previous data, High Temp.–High Press. 22 (1990) 613–621.
[31] Viscosity and density of over 40 lubricating fluids of known composition at pressures to 150000 psi and temperatures to 425 F. ASME Report. New York: American Society of Mechanical Engineers; 1953.